The Effect of Boundary Conditions on Performance Prediction Model Results for Tidal Turbines

N.E. Turner[1] and A. Owen[2]

[1] CRE+E,
School of Engineering, The Robert Gordon University,
Schoolhill, Aberdeen, AB10 1FR, United Kingdom
E-mail: prs.turner@rgu.ac.uk
[2] CRE+E
School of Engineering, The Robert Gordon University,
Schoolhill, Aberdeen, AB10 1FR, United Kingdom
E-mail: a.owen@rgu.ac.uk

Abstract

Aerodynamic models are typically used to model tidal turbines but the differences between wind and tidal turbines are such that these models may not accurately represent the performance of a tidal turbine. Aerodynamic models assume free flow whereas in a tidal channel the channel boundaries are likely to have an effect on turbine performance. Models for flows with three different boundary conditions have been developed in order to demonstrate how significant the effect of the boundaries is. The first model is the classic aerodynamic model, the second considers flow in which all the boundaries are rigid and the third considers a channel where the free surface can deform. The effect of channel area to turbine area on performance has been investigated using these models. The results from the models indicate that the boundary conditions assumed in the model have a significant effect on the predicted performance of the turbine. The difference between the model results increases as the tip speed ratio increases and as the ratio of channel area to turbine area is reduced. The model results suggest that for realistically sized devices in actual tidal channels, aerodynamic models will not provide an accurate prediction of the performance.

Keywords: Blade Element momentum, Performance prediction modelling, tidal turbine

Nomenclature

a'	= tangential interference factor
a	= axial interference factor
A_o	= upstream streamtube area(m)
A	= swept area of turbine (m^2)
A_2	= streamtube area in far downstream region (m^2)
C	= blade chord (m)
C_D	= Drag coefficient
C_L	= Lift coefficient
I	= iteration number
N	= number of blades
P_∞	= free stream pressure (Pa)
P_D	= pressure at upstream side of disc (Pa)
P_2	= pressure at downstream region (Pa)
q	= torque acting per unit length of blade (N)
R	= blade radius (m)
r	= local radius (m)
R_r	= root radius of turbine blades (m)
T	= thrust force acting on actuator disc (N)
u_∞	= freestream velocity (m/s)
u_{1o}	= flow velocity outside streamtube at actuator disc (m/s)
u_{2o}	= flow velocity outside streamtube in far downstream region (m/s)
u_{2s}	= downstream flow velocity in streamtube, (m/s)
u_{1o}	= velocity at actuator disc outside streamtube (m/s)
u	= actuator disc velocity (m/s)
W	= resultant relative velocity (m/s)
y	= channel depth (m)
Δy	= deflection of free surface (m)
ΔP	= pressure change across actuator disc (Pa)
z	= channel width (m)
α	= angle of incidence
β	= pitch angle of blade
λ	= tip speed ratio
ρ	= density of fluid (kg/m^3)
ϕ	= the angle between W and the plane of the actuator disc
Ω=	angular velocity of turbine (rad/s)

1 Introduction

Mathematical models are powerful tools in the development of tidal turbines since they allow design parameters to be optimised more rapidly and at a lower cost than scale model testing. Tidal turbines are typically modelled using the blade element momentum or vortex models developed for wind turbines [1-7] however there are a number of significant differences between extracting energy from the wind and extracting energy from tidal flows. The differences between wind and tidal turbines include the Reynolds number of the flow, the possibility of cavitation occurring, different stall characteristics, the presence of a free surface, and wave motion. It should also be noted that whilst the flow through a wind turbine is constrained by the ground it is free above and to the sides of the turbine. The flow through a tidal turbine is constrained between the channel bed and the free surface. In narrow channels the sides walls of the channels may also have an effect. These differences are likely to affect the performance of the turbine and hence limit the applicability of aerodynamic models to tidal turbines.

Models have been developed that build on the basic aerodynamic models by considering wave loads [8], unsteady loads [9], shrouded turbines and other differences in turbine geometry [10], cavitation [11] and the tidal velocity profile [12]. The effect of the channel boundaries on the performance of turbines has received little attention. Garret and Cummins investigated the effect of using an isolated turbine or a partial fence on the extractable power in a tidal channel [13]. In this model it was assumed that the turbines were ideal so the power generated by a turbine was equal to the product of the force acting on the actuator disc and the flow velocity at the actuator disc. In a real turbine the drag forces acting on the blades contribute to the force acting on the actuator disc without contributing to the power generated by the turbine and so the power generated is lower. This work provides an excellent insight into how the obtainable power varies with the fraction of the cross section taken up by turbines but does not directly allow the effect of the ratio of turbine cross section to channel cross section on the generated power of an actual device to be investigated.

Whelan et al used actuator strip theory to calculate the blockage effect due to the free surface for an array of tidal stream turbines [14]. This allowed them to develop a correction to the wake induction factor for use in Blade Element Momentum codes. The deforming boundary model below is based on this modelling work however a different solution method is used. The graphical solution method provides greater understanding as it shows how the variation of momentum and blade element forces with actuator disc velocity combine to determine the performance of the turbine. A case study is also presented below which allows the significance of the blockage effects to be understood when considering realistically sized devices in actual tidal channels.

2 Models

In order to investigate whether or not the channel boundaries are likely to have an effect on turbine performance three simple models with different boundary conditions are presented below. The first is the classic aerodynamic model in which the flow is unbounded; the second models a flow that is constrained by rigid boundaries on all sides; and in the third the flow is constrained by rigid boundaries on three sides and a free surface on the fourth. The deformation of the free surface can vary along the length of the channel but is constant across the width of the channel for any given section.

The models are based on the blade element momentum theory model with adjustments made for the differences in downstream pressure and flow area caused by the different boundary conditions. In blade element momentum models the force acting on the turbine blades is related to the change in the fluid momentum. The notation used in the models is shown in Figure 1. It should be noted that the pressures are taken to be the absolute pressure + ρgh.

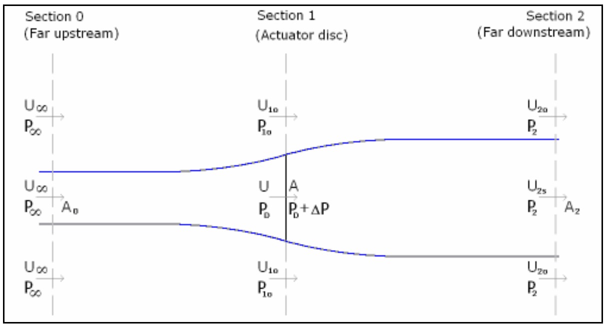

Figure 1: definition of flow velocities and pressures.

Aerodynamic model

The aerodynamic model considered is one of the blade element momentum model for a horizontal axis turbine presented by Sharpe in [15]. A flow chart showing calculation procedure is shown in Figure 2.

Once the values for the axial and tangential interference factors have converged the torque acting per unit length of blade can be calculated using Equation 1. The torque acting on the complete rotor is given by Equation 2 and the power coefficient by Equation 3.

$$q = 0.5\rho W^2 Nc\left(C_L \cos\phi - C_D \sin\phi\right)r \qquad (1)$$

$$Q = \int_{Rr}^{R} q\,dr \qquad (2)$$

$$C_p = \frac{Q\Omega}{0.5\rho u_\infty^2 A} \qquad (3)$$

This model has been applied to a turbine of the dimensions modelled and tested by Batten et al [12]. In Figure 3 the output of this model is plotted with the reported output from Batten’s model. There is some difference between the model results and the verification model results. This difference is likely to be due to errors in the aerofoil lift and drag coefficient data used. The coefficient data used was estimated from graphs of lift and drag coefficient variation with angle of attack presented in [12]. These graphs apply to a single, unspecified, flow Reynolds number but the data has been used for the whole range of Reynolds numbers which will introduce errors. The agreement between the model and the verification model output was felt to be sufficiently good for the model to be used in the investigation of the effect of the boundary conditions on the performance of the turbine.

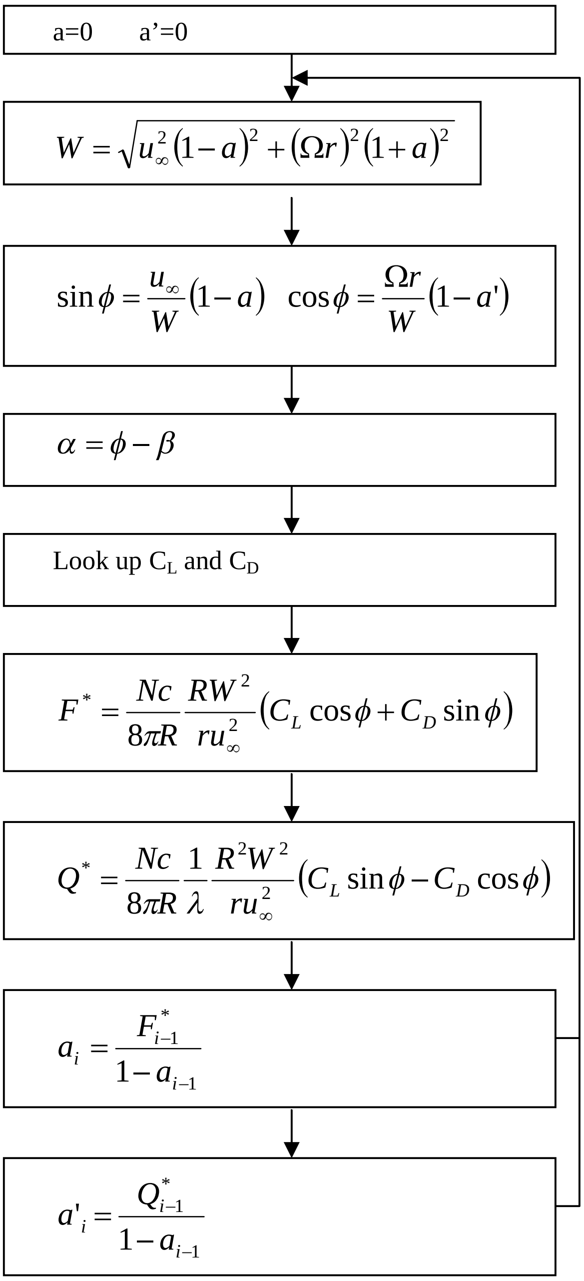

Figure 2: flow chart showing calculation procedure for blade element momentum model.

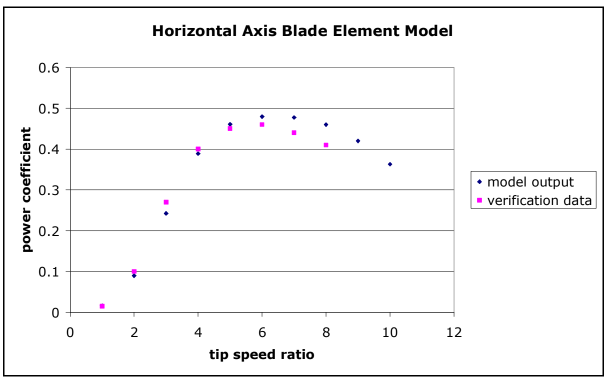

Figure 3: Model results plotted with verification data.

Flow Constrained Between Rigid Boundaries

The flow in a tidal channel is more constrained than the free flow assumed in the aerodynamic model. The simplest constrained flow to model is a flow constrained on all sides by rigid boundaries. This is equivalent to model testing in a closed section wind tunnel where blockage effects can increase the performance of a turbine [16]. For an open channel flow in a uniform channel, the channel area can be taken to be constant if the Froude number is small which is typically the case for tidal channels [13]. The assumption of constant cross sectional area simplifies the modelling since the cross sectional area of the channel is known at all sections.

Applying Bernoulli's equation in the valid regions yields an expression for the pressure change across the actuator disc.

$$\Delta P = P_2 - P_\infty + \frac{1}{2}\rho\left(U_{2s}^2 - U_\infty^2\right) \tag{4}$$

Applying Bernoulli's equation along the surface gives:

$$P_\infty + \frac{1}{2}\rho U_\infty^2 = P_2 + \frac{1}{2}\rho U_{2o}^2 \tag{5}$$

Rearranging to make $P_2 - P_\infty$ the subject gives:

$$P_2 - P_\infty = \frac{1}{2}\rho\left(U_\infty^2 - U_{2o}^2\right) \tag{6}$$

Substituting Equation 6 into Equation 4 gives:

$$\Delta P = \frac{1}{2}\rho\left(U_{2s}^2 - U_{2o}^2\right) \tag{7}$$

The pressure change across the actuator disc can be related to the force acting on the actuator disc by:

$$\Delta P = \frac{T}{A} \tag{8}$$

Combining Equation 7 and Equation 8 gives:

$$T = \frac{1}{2}\rho A\left(U_{2s}^2 - U_{2o}^2\right) \tag{9}$$

Conservation of mass gives:

$$AU = A_2 U_{2s} \tag{10}$$

$$\left(yz - A_2\right)U_{2o} = yzU_\infty - AU \tag{11}$$

Equation 10 and Equation 11 allow Equation 9 to be expressed in terms of the far downstream streamtube area and the velocity of the flow through the actuator disc:

$$T = \frac{1}{2}\rho A\left[\left(\frac{Au}{A_2}\right)^2 - \left(\frac{yzu_\infty - Au}{yz - A_2}\right)^2\right] \qquad (12)$$

Applying conservation of linear momentum to the flow gives:

$$T = A_2\rho u_{2s}(u_{2s} - u_\infty) + (yz - A_2)\rho u_{2o}(u_{2o} - u_\infty) + yz(P_2 - P_\infty) \qquad (13)$$

Substituting Equation 6, Equation 10 and Equation 11 into this expression gives:

$$T = \rho Au\left(\frac{Au}{A_2} - u_\infty\right) + \rho\left(\frac{yzu_\infty - Au}{yz - A_2} - u_\infty\right)(yzu_\infty - Au) + \frac{1}{2}\rho yz\left(u_\infty^2 - \left(\frac{yzu_\infty - Au}{yz - A_2}\right)^2\right) \qquad (14)$$

Equation 12 and Equation 14 can be used to calculate the thrust force acting on the actuator disc (T) for a given value of actuator disc velocity (u).

Another equation for T in terms of u can be obtained by summing the axial forces acting on the blade elements. An additional iterative procedure is needed to find the tangential interference factor for each blade element. The calculation procedure outlined in Figure 5 can be used to calculate the sum of the thrust forces acting on the blade elements for any given values for the u and tip speed ratio. The blade element forces vary with tip speed ratio but are independent of channel area.

Plotting the variation of T with u from both the momentum equations and the blade element equations allows a solution to be found for T and u for a given values of tip speed ratio and the ratio of channel area to turbine actuator disc area. An example of a plot of blade element forces and momentum forces is shown in Figure 4. Once u is known, the power coefficient of the turbine can be calculated using Equation 1, Equation 2 and Equation 3.

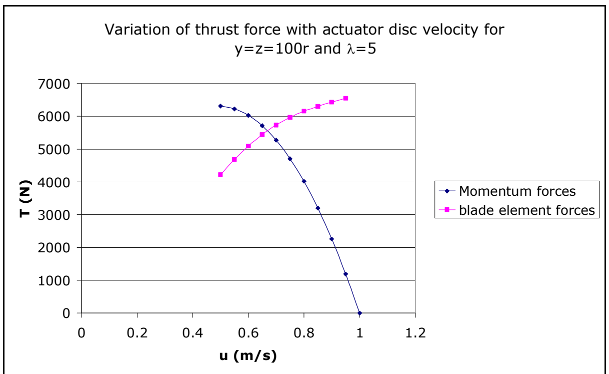

Figure 4: Example of graphical solution for T and u.

Flow constrained by rigid boundaries and a deforming free surface

The difference in surface elevation of the far upstream and downstream sections may be negligible, however a major shortcoming of the rigid boundaries model presented above is that it does not accurately represent the pressure distribution in an open channel flow. In an open channel the pressure at the interface between the flow and the air is atmospheric. In the rigid boundaries model the pressure at the surface in the far downstream region was not equal to atmospheric pressure. By allowing the free surface to deform, a more realistic far downstream pressure distribution can be modelled.

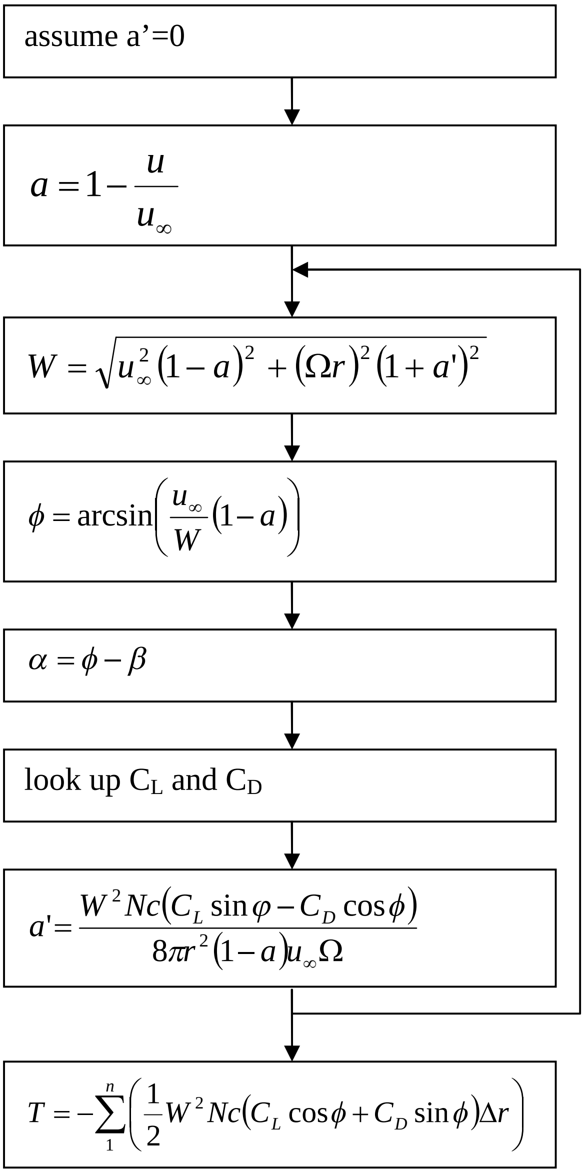

Figure 5: Iterative calculation procedure used to find the thrust force acting on the actuator disc from the blade element forces.

Applying Bernoulli's equation in valid regions of the streamtube gives:

$$\Delta P = \rho g\Delta y + \frac{1}{2}\rho\left(u_{2s}^2 - u_\infty^2\right) \qquad (15)$$

Substituting Equation 8 into Equation 15gives

$$T = \rho g A \Delta y + \frac{1}{2}\rho A\left(u_{2s}^2 - u_\infty^2\right) \tag{16}$$

Bernoulli's equation applied along the surface yields:

$$\frac{1}{2}\rho\left(u_\infty^2 - u_{2o}^2\right) = \rho g \Delta y \tag{17}$$

Applying conservation of linear momentum gives:

$$\begin{aligned} T &= A\rho u\left(u_{2s} - u_\infty\right) + \left(zy - A_o\right)\rho u_\infty\left(u_{2o} - u_\infty\right) \\ &-\frac{1}{2}\rho g z\left(y^2 - (y+\Delta y)^2\right) \end{aligned} \tag{18}$$

Continuity:

$$\left(yz - A_o\right)u_\infty = \left(z(y+\Delta y) - A_2\right)u_{2o} \tag{19}$$

$$u_\infty A_o = uA \tag{20}$$

$$uA = u_{2s} A_2 \tag{21}$$

Substituting the continuity equations into Equation 16, Equation 17 and Equation 18 gives:

$$\Delta y = \frac{1}{2g}\left[u_\infty^2 - \left(\frac{yzu_\infty - uA}{z(y+\Delta y) - A_2}\right)^2\right] \tag{22}$$

$$T = \rho g \Delta y A + \frac{1}{2}\rho A\left[\left(\frac{uA}{A_2}\right)^2 - u_\infty^2\right] \tag{23}$$

$$\begin{aligned} T &= A\rho u\left(\frac{uA}{A_2} - u_\infty\right) \\ &+ \left(zy - \frac{uA}{u_\infty}\right)\rho u_\infty\left(\frac{zyu_\infty - uA}{z(y+\Delta y) - A_2} - u_\infty\right) \\ &-\frac{1}{2}\rho g z\left(y^2 - (y+\Delta y)^2\right) \end{aligned} \tag{24}$$

This system of equations can be solved to give the variation of T with u. An iterative procedure was used to find the variation of Δy with A_2 from Equation 22 and these values used in the numerical solution of Equation 23 and Equation 24. The blade element forces and the value of u which satisfies both the blade element and momentum equations can be calculated in the manner described in the rigid boundaries section.

3 Results

These models have been applied to a 4m diameter turbine with three tapered and twisted NACA 0018 section blades. The root radius of the turbine is 0.105m. Each blade was represented by 10 blade elements. The chord lengths and pitch distribution of the blade elements are presented in Table 1.

r (m)	c (m)	pitch distribution (°)
0.19975	0.401	7.348
0.38925	0.376	0.3389
0.57875	0.351	-4.812
0.76825	0.325	-8.423
0.95775	0.300	-10.81
1.14725	0.274	-12.30
1.33675	0.249	-13.21
1.52625	0.224	-13.85
1.71575	0.198	-14.56
1.90525	0.173	-15.62

Table 1: radius, chord length and pitch distribution of the blade elements.

The pitch angle of the blade element, β, is equal to the pitch distribution plus the hub pitch angle.

The rigid boundaries and deforming boundary models were applied to square channels with side lengths of 4R, 10R, 20R, 100R and 10000R. These results are plotted with the curve from the aerodynamic model in Figure 6. The maximum power coefficient for two of the curves in Figure 6 is greater than the Betz limit. The Betz limit is derived for a turbine in free flow so for cases where blockage is significant the maximum power coefficient can actually exceed the Betz limit. The two curves which exceed the Betz limit are for cases where the ratio of turbine area to channel area is high and so the blockage effect is large.

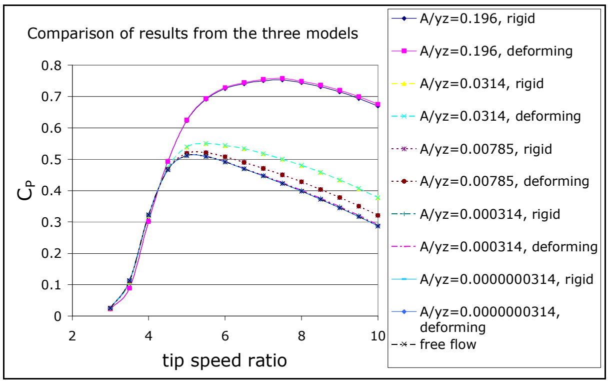

Figure 6: comparison of results from the three models.

It can be seen from Figure 6 that the difference in the results from all three models decreases as the channel area is increased. The difference between the deforming free surface and rigid boundaries models and the free flow model is very small for the channels with y=z=100r (A/yz= 0.000314) and y=z=1000r (A/yz=0.0000000314). The results from the deforming free surface and rigid boundaries models is very similar with a difference between the two data sets only apparent for the smallest channels.

For the smaller channel areas the peak of the power coefficient curve is shifted up and to the right. For tip speed ratios less than 4 the power coefficient values calculated using the rigid boundaries and deforming free surface models are below those of the free flow model. In this region, the region before the power coefficient of the free flow starts to peak, the results are less dependant on channel area.

Case study- Sound of Islay

The sound of Islay is the channel between the islands of Islay and Jura which lie off the West coast of Scotland (Figure 7). This area has an energetic tidal stream resource and is also closer to regions of demand than much of Scotland's tidal stream resource so it is an ideal region for initial commercial tidal stream power development. One of the narrower sections of the sound of Islay has a width of 900m and a cross sectional area of 21685m^2. This section, labelled section 11 in Figure 8, is an East-West section across the channel at Port Askaig. The models developed above will be applied to this section of the channel.

Figure 7: Sound of Islay.

The section of channel will be represented by a rectangular section with width 900m and depth 24m (the average depth of the channel at the section). The Seagen device installed in Stranford Lough has two 16m diameter rotors [15]. This section has a depth of three times the radius of the Seagen device.

The models have been applied to rotors with diameters of 16m and 12m. For the 16m diameter rotor y=3r and z≈112r and for the 12m diameter rotor y=4r and z=150r. Figure 9 and Figure 10 show the deforming free surface model results plotted with the free flow results for a number of channel widths for channel depths of 3r and 4r. From Figure 9 it is apparent that for a 16m diameter turbine, the results have not converged to those of the free flow model for a channel width of either 800m or 1200m. Since the curve for a 900m wide channel will lie between the 800m and 1200m wide channel curves, the use of an aerodynamic model to represent a 16m diameter turbine in this section would lead to errors in the predicted performance. Similarly for the 12m diameter rotor the deforming free surface model for a 900m wide channel has not converged to the free flow model and so an aerodynamic model does not accurately represent this case either.

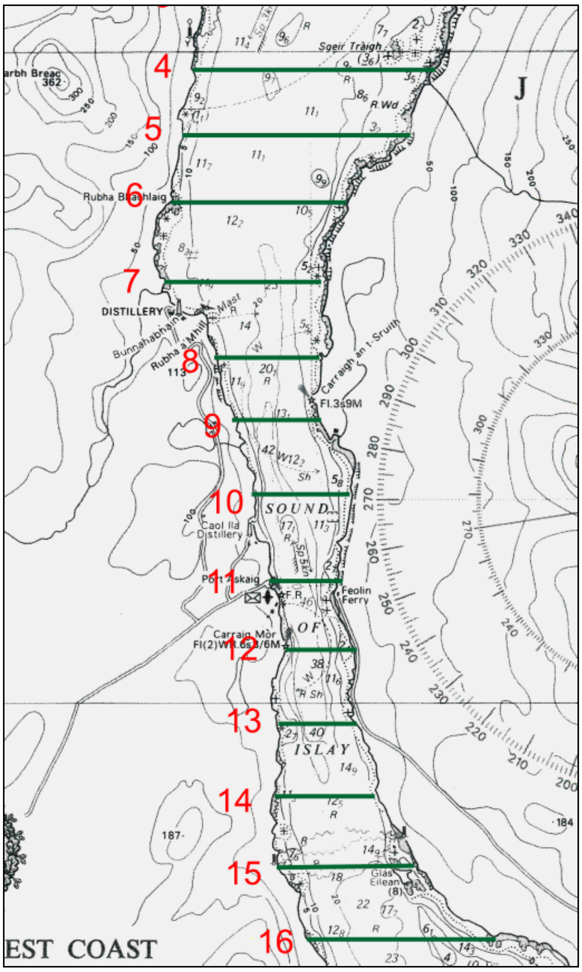

Figure 8: Position of section used as example in case study.

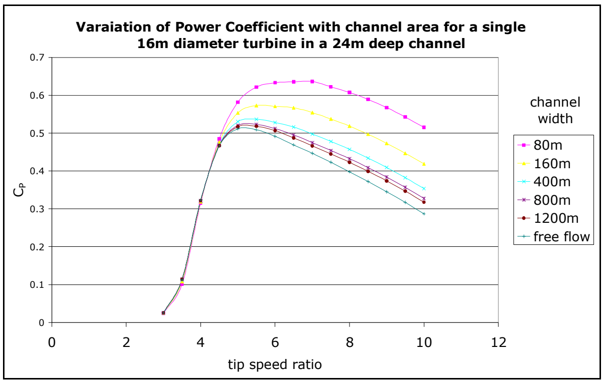

Figure 9: variation of power coefficient with channel area for 16m diameter turbine.

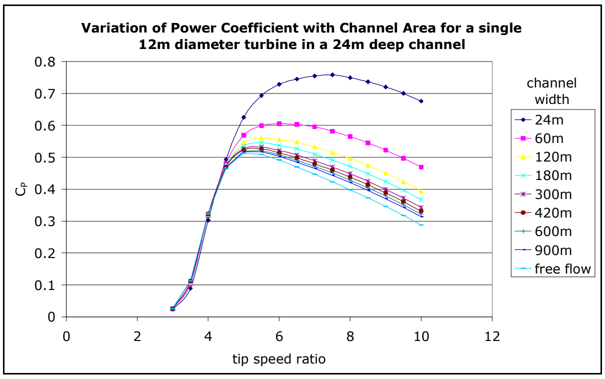

Figure 10: variation of power coefficient with channel area for 12m diameter turbine.

4 Conclusions

Three models have been presented which predict the performance of turbines in flows with different boundary conditions. The model with rigid boundaries was found to give similar results to the model in which the free surface could deform by a constant height over the width of the channel except for channels which were very small in relation to the turbine. The results from the rigid boundary and deforming free surface models converged towards those from the free flow model as the size of the channel was increased. The difference between the results from all the models was greatest at the higher tip speed ratios. When the deforming free surface model was applied to a single realistically sized turbine in a section of a real tidal channel it was found that there was a significant difference between the results of this model and the free flow model, implying that the use of aerodynamic models to represent tidal turbines will lead to errors. It is also unlikely that only a single device would be installed in a channel, so the ratio of channel area to device area will be even smaller and the difference between the two models even more pronounced.

The models presented here are very simple models and have a number of limitations. The models assumed that the tidal channels were uniform and rectangular and that the flow was frictionless. In the deforming boundary model it was assumed that the deformation of the free surface was constant across the width of the channel. These conditions do not occur in actual tidal channels, so none of the models can be used to accurately predict the performance of a turbine. However the models do demonstrate that the boundary conditions used in a model do have a significant effect on the results for realistically sized devices and channels, even if they cannot accurately quantify the effect of the boundaries.

The models developed do not take into account the distance between the turbine and the free surface. Akwensivie [18] demonstrated using CFD modelling that the wake of the turbine changed with distance of the turbine from the surface. This change in wake geometry also implies a change in turbine performance. For the performance prediction models to accurately model tidal turbines they also need to be able to take into account the effects of surface proximity.

References

[1] Bahaj, A.S., Molland, A.F., Chaplin, J.R. and Batten, W.M.J. Power and thrust measurements of marine current turbines under various hydrodynamic flow conditions in a cavitation tunnel and a towing tank. *Renewable Energy*, 2007, 32(3), 407-426.

[2] Bahaj, A.S. and Myers, L.E. Fundamentals applicable to the utilisation of marine current turbines for energy production. *Renewable Energy*, 2003, 28(14), 2205-2211.

[3] Camporeale, S.M. and Magi, V. Streamtube model for analysis of vertical axis variable pitch turbine for marine currents energy conversion. *Energy Conversion and Management*, 2000, 41(16), 1811-1827.

[4] Edinburgh Designs. Variable pitch foil vertical axis tidal turbine. (DTI T/06/00234/00/REP, 2006).

[5] Wang, L.B., Zhang, L. and Zeng, N.D. A potential flow 2-D vortex panel model: Applications to vertical axis straight blade tidal turbine. *Energy Conversion and Management*, 2007, 48(2), 454-461.

[6] J A Clarke, G.C., A D Grant, and C M Johnstone. Design and testing of a contra-rotating tidal current turbine. *J. Power and Energy*, 2007, 221.

[7] R F Nicholls-Lee, S.R.T., S W Boyd. Simulation Based Optimisation of Marine Current Turbine Blades. *7th International Conference on Computer and IT Applications in the Maritime Industries (COMPIT'08)*Liège, 2008).

[8] Barltrop, N., Varyani, K.S., Grant, A., Clelland, D. and Pham, X.P. Investigation into wave–current interactions in marine current turbines. *J. Power and Energy*, 2007, 221.

[9] Grant, A.G., Johnstone, C.M. and McCombes, T. Unsteady Hydrodynamic Modelling of Rotor Systems Used in Marine Current Turbines. *10th World Renewable energy Congress*Glasgow, 2008).

[10] Robinson, E. and Byrne, G. Methodology for Modeling Tidal Turbine Characteristics. *OCEANS 2008 MTS/IEEE QUEBEC Conference & Exhibition*Quebec, 2008).

[11] Batten, W.M.J., Bahaj, A. S., Molland, A. F., Chaplin, J. R. Hydrodynamics of marine current turbines. *Renewable Energy*, 2006, 31(2), 249-256.

[12] Batten, W.M.J., Bahaj, A.S., Molland, A.F. and Chaplin, J.R. The prediction of the hydrodynamic performance of marine current turbines. *Renewable Energy*, 2008, 33(5), 1085-1096.

[13] Garrett, C., Cummins P. The efficiency of a turbine in a tidal channel. *J. Fluid Mech.*, 2007, 588, 243-251.

[14] Whelan, J., Thomson, M.D., Graham, J.M.R. and Peiro, J. Modelling of free surface proximity and wave induced velocities around a horizontal axis tidal stream turbine. *7th European Wave and Tidal Energy Conference*Porto, Portugal, 2007).

[15] Sharpe, D.J. Wind Turbine Aerodynamics. In Freris, L.L., ed. *Wind Energy Conversion Systems*, pp. 55-118 (Prentice Hall, 1990).

[16] Pope, A. and Harper, J. *Low-speed wind tunnel testing* (Wiley, 1966).

[17] Marine Current Turbines.

[18] Akwensivie, F. In the Wake of a Marine Current Turbine. (The University of Strathclyde, 2004).